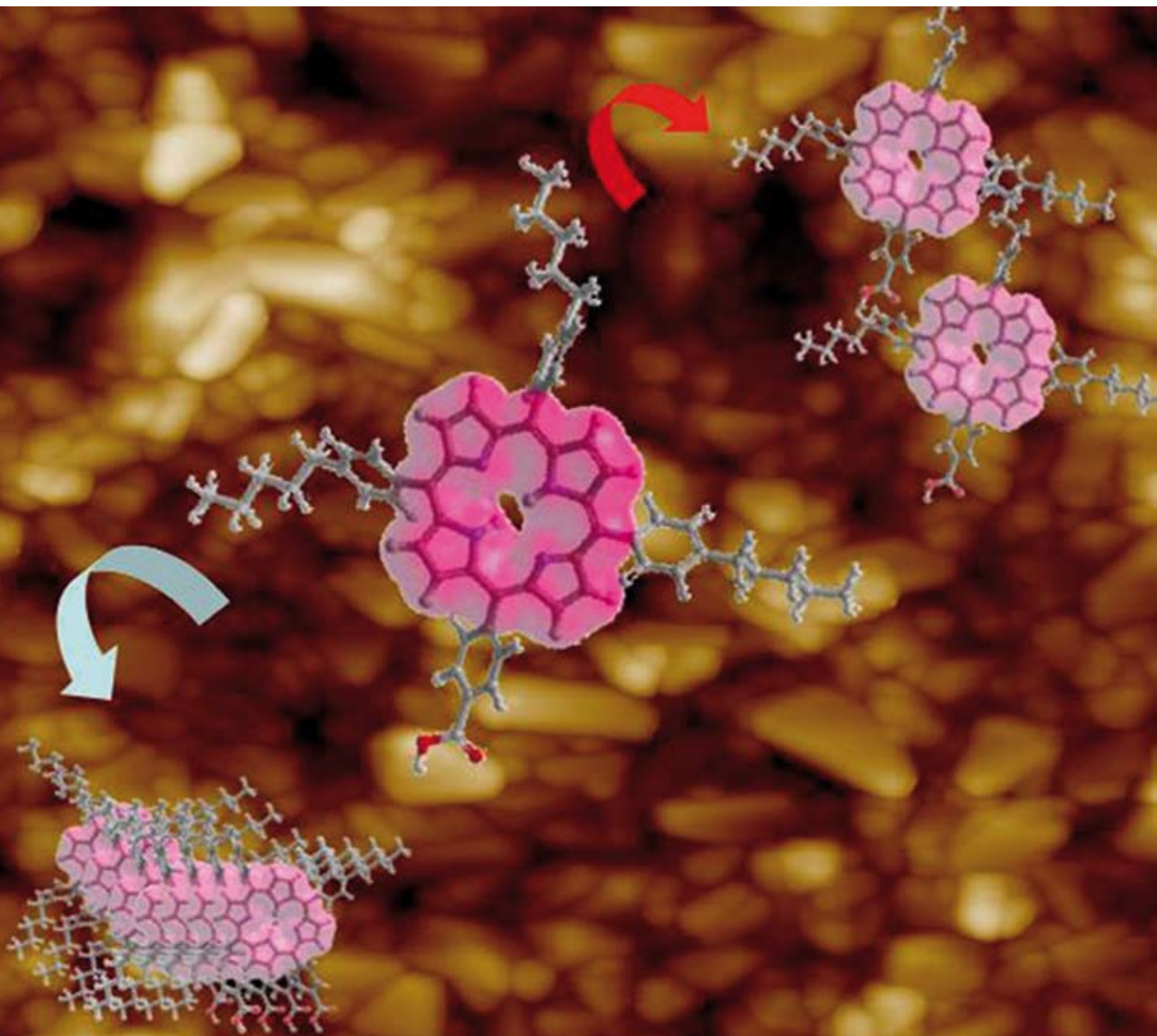


Journal of Materials Chemistry

www.rsc.org/materials

Volume 18 | Number 14 | 14 April 2008 | Pages 1605–1712

Downloaded by Brown University on 16 January 2013
Published on 19 February 2008 on http://pubs.rsc.org | doi:10.1039/B717081E



ISSN 0959-9428

RSC Publishing

PAPER

Emilio Palomares *et al.*
The role of para-alkyl substituents on
meso-phenyl porphyrin sensitised
TiO₂ solar cells: control of the $e_{\text{TiO}_2}^-$ /
electrolyte⁺ recombination reaction

HIGHLIGHT

He Tian and Yanli Feng
Next step of photochromic switches?

The role of *para*-alkyl substituents on *meso*-phenyl porphyrin sensitised TiO₂ solar cells: control of the e_{TiO₂}/electrolyte⁺ recombination reaction

Amparo Forneli,^a Miquel Planells,^a Maria Angeles Sarmentero,^a Eugenia Martinez-Ferrero,^a Brian C. O'Regan,^b Pablo Ballester^{*ac} and Emilio Palomares^{*ac}

Received 5th November 2007, Accepted 29th January 2008

First published as an Advance Article on the web 19th February 2008

DOI: 10.1039/b717081e

We aim to investigate the effect of adding hydrophobic alkyl chains substituents to unsymmetrical free base tetra-phenyl porphyrins used for the preparation of dye sensitised solar cells (DSSC). We have used two different unsymmetrical *meso*-tetraphenyl substituted free base porphyrins attending to two objectives: (1) to observe how the substitution of three *para* positions of the *meso*-phenyl groups with hydrophobic alkyl chains influences the formation of molecular aggregates onto the semiconductor nanoparticles and (b) to deduce the influence that the substitution exerts over the e_{TiO₂}/electrolyte⁺ recombination reaction in operating devices. To achieve these goals we have focussed on the study of the electron transfer processes that take place at the different interfaces of the photovoltaic device using electrochemistry, steady-state and time resolved spectroscopic techniques.

Introduction

Since the seminal paper of O'Regan and Grätzel,¹ about the use of mesoporous semiconductor metal oxides sensitised with a monolayer of photo-active molecules to convert solar irradiation into electrical power, there has been an intensive effort towards the synthesis of efficient dyes that could push the efficiency above 10%. In fact, this has already been achieved by several groups using ruthenium dyes,² where the optical and electrochemical properties have been designed to achieve optimal electron injection into the semiconductor, slow back-electron transfer kinetics and efficient regeneration of the light-induced oxidized molecule by the solution electrolyte.

The electron transfer (ET) reactions taking place at the different interfaces of the dye sensitized solar cell device have an extraordinary resemblance to the ET reactions that occur at the photosynthetic reaction centre (PSC) of several bacteria and plants.³ In fact, an extensive number of scientists have synthesized dyads and triads based on porphyrins, or even more complex structures such as dendrimers, to mimic, in solution, the ET processes at the PSC.⁴ Only recently, the use of such biological dyes, *i.e.* Zn-porphyrins, in molecular photovoltaic devices have given impressive light-to-energy efficiencies when irradiated at 1 sun⁵ (100 mW cm⁻²) although free-base porphyrins have only reached efficiencies higher than 5% but at much lower light intensities (1.5 mW cm⁻²).⁶ Several authors have assigned the low performance of porphyrin based devices to the dye desorption process and to the formation of molecular aggregates onto the surface of the nanoparticles.^{6a,7} To avoid or limit the aggregation inconvenience we have decided to explore

the use of alkyl chain substituents in the porphyrin structure. Other authors, using ruthenium bis-thiocyanate polypyridyl dyes, have already used such a strategy in order to increase not only the device efficiency but also the stability of the photovoltaic cells under illumination.⁸ However, there is still some controversy about the effect of the hydrophobic alkyl chains on the control of the electron recombination dynamics between the photo-injected electrons at the semiconductor metal oxide and the electrolyte.⁹ In principle, porphyrins, due to their tendency to form aggregates, are ideal candidates to study whether the presence of hydrophobic alkyl chain substituents in their molecular structure not only inhibits or reduces the formation of molecular aggregates, but also creates a compact hydrophobic layer at the nanoparticle surface that may increase the distance with the I⁻/I₃⁻ redox electrolyte and, therefore, slow the back electron transfer reaction. Hence, we decided to use such "biological like" dyes for our study.

As molecular sensitizers we synthesised the unsymmetrical porphyrins illustrated in Fig. 1.

Experimental

Materials and reagents

All reagents were purchased from Aldrich and the solvents from SDS. All were used as received without further purification, except pyrrole which was distilled under vacuum prior to use.

Synthesis of porphyrins

The methodology for the synthesis of unsymmetrical free base porphyrins has been described by Lindsey *et al.*¹⁰ Scheme 1 illustrates the synthetic steps for the preparation of **FbP1** and **FbP2**.

Synthesis of 4-pentylbenzaldehyde

4-Pentylbenzene (25 mL; 0.145 mol) and 20.4 g of hexamethylenetetramine (0.145 mol) were added in a round bottom flask

^aInstitute of Chemical Research of Catalonia (ICIQ), Avda. Països Catalans, 16 Tarragona, Spain. E-mail: epalomares@icq.es; pballester@icq.es; Fax: +34 977 920 224; Tel: +34 977 920 241

^bCentre for Electronic Materials and Devices, Dept. Chemistry, Imperial College of London, London, UK, SW7 2AZ

^cCatalan Institution for Research and Advanced Studies (ICREA), Spain

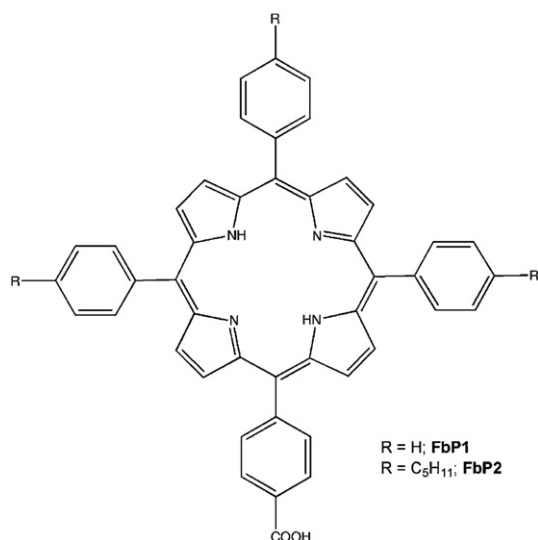
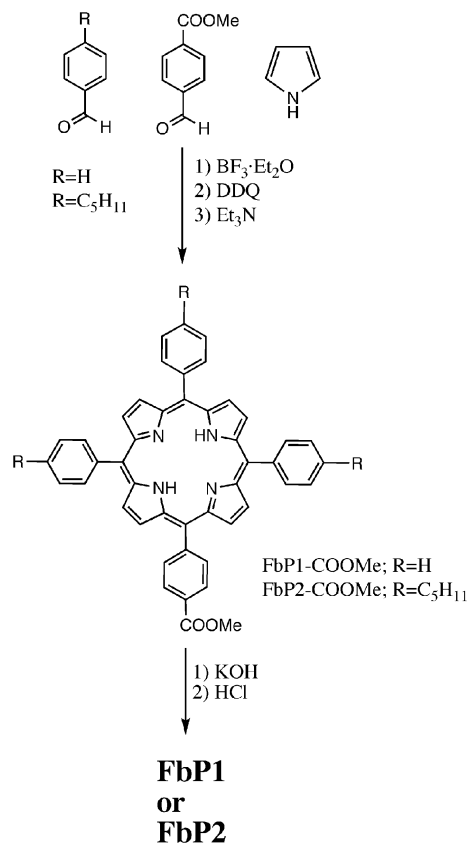


Fig. 1 Molecular structures of **FbP1** and **FbP2**.



Scheme 1 Synthesis route to **FbP1** and **FbP2**.

to 250 mL of TFA (trifluoroacetic acid). The mixture was heated to 100 °C for 12 h. Then, TFA was removed under vacuum and 250 mL of ice-water were added to the concentrate. Under stirring, sodium carbonate was added to the solution until a pH value ~8 was achieved. Diethyl ether was added and the organic layer was separated and washed with water. The organic layer was dried over sodium sulfate, filtered and concentrated

under vacuum. Finally, the product was purified by distillation of the residue under diminished pressure (130 °C, 1 mbar). The compound was isolated as a colourless liquid in 39% yield.

¹H-NMR (400 MHz, CDCl₃) δ_H: 9.96 (1 H, s); 7.79 (2 H, d, *J* = 8.0 Hz); 7.32 (2 H, d, *J* = 8.0 Hz); 2.67 (2 H, t, *J* = 8.0 Hz); 1.64 (2 H, m); 1.33 (2 H, m); 1.32 (2 H, m); 0.89 (3 H, t, *J* = 6.8 Hz).

¹³C-NMR (400 MHz, CDCl₃) δ_C: 191.93; 150.45; 134.43; 129.86; 129.07; 36.17; 31.42; 30.75; 22.48; 13.97.

Synthesis of 5-(4-carboxyphenyl)-10,15,20-trisphenylporphyrin (**FbP1**) and 5-(4-carboxyphenyl)-10,15,20-tris(4-pentylphenyl)porphyrin (**FbP2**)

Methyl 5-formylbenzoate (1 g; 6.1 mmol), the appropriate aldehyde (either 0.95 mL of benzaldehyde (9.1 mmol) or 1.45 g of 4-pentylbenzaldehyde (9.1 mmol)) and 0.95 mL of freshly distilled pyrrole (15.2 mmol) were added to a solution consisting of 530 mL of dichloromethane and 4 mL of ethanol. The resulting solution was stirred under argon for 10 min. The reaction mixture was protected from light and 0.69 mL of boron trifluoride dietherate (6.1 mmol) was added. The solution was stirred for 60 min. Subsequently, 3.11 g of 2,3-dicyano-5,6-dichloropara-benzoquinone (15.2 mmol) were added and the reaction was stirred for another 90 min. After, the reaction was quenched by the addition of 3 mL triethylamine. The solvent was removed under vacuum and the crude was purified by column chromatography on silica gel using a 1 : 1 hexane–dichloromethane solvent mixture. The mono-carboxymethylporphyrins were isolated as purple solids in 10% (**FbP1-COOMe**) and 7.5% (**FbP2-COOMe**) yields. Finally, the ester group was hydrolyzed to the carboxylic acid anchoring group. In brief, 90 mg of mono-carboxymethylporphyrin **FbP1-COOMe** (0.14 mmol) or **FbP2-COOMe** (0.1 mmol) were added to a mixture of 8 mL of THF (tetrahydrofuran) and 2 mL of 2 M aqueous KOH. The reaction was stirred for 14 h at 90 °C. After, the THF was removed under vacuum and 80 mL of water were added to the resulting concentrate. The pH of the solution was adjusted to pH 4.0–5.0 using a solution of HCl (2 M), followed by the addition of 100 mL of chloroform. The organic layer was separated, washed with water, dried over sodium sulfate and filtered. The organic solvent was removed under vacuum, giving the pure free base monocarboxylic acid porphyrins as purple solids with 95% yield in both cases. The porphyrins were dried overnight before being used in the construction of the devices.

FbP1: ¹H-NMR (400 MHz; CHCl₃) δ_H: 8.77 (8 H, m); 8.37 (2 H, d, *J* = 7.9 Hz); 8.23 (2 H, d, *J* = 7.9 Hz); 8.14 (6 H, m); 7.70 (9 H, m); –2.89 (2 H, br s).

ESI/MS (*m/z*): [M + H]⁺ = 659.2442 (calc. M for C₄₅H₃₀N₄O₂ = 658.2369).

FT-IR (cm⁻¹): 2952, 2922(w), 2852(w), 1684, 1606, 1556, 1422, 1288, 797, 722, 700.

FbP2: ¹H-NMR (400 MHz, CDCl₃) δ_H: 8.92 (2 H, d, *J* = 4.8 Hz); 8.89 (4 H, s); 8.80 (2 H, d, *J* = 4.8 Hz); 8.51 (2 H, d, *J* = 8.0 Hz); 8.36 (2 H, d, *J* = 8.0 Hz); 8.13 (6 H, d, *J* = 8.0 Hz); 7.59 (6 H, d, *J* = 8.0 Hz); 2.98 (6 H, t, *J* = 8.0 Hz); 1.95 (6 H, m); 1.56 (12 H, m); 1.08 (9 H, t, *J* = 6.8 Hz); –2.73 (2 H, br s).

MALDI/MS (*m/z*): [M – H][–] = 867.4623 (calc. M for C₆₀H₆₀N₄O₂ = 868.4716).

FT-IR (cm⁻¹): 2953, 2922(s), 2852(s), 1688, 1606, 1420, 1278, 1178(s), 965(s), 797, 729.

Titanium nanoparticles synthesis

TiO₂ anatase nanoparticles were prepared as previously reported by Palomares *et al.*¹¹ Titanium isopropoxide (40 mL, 0.13 mol) was added to glacial acetic acid (9.12 g) under stirring. The resulting solution was cooled in an ice-bath and 240 mL of 0.1 M HNO₃ were added under vigorous stirring. The mixture was heated at 80 °C for 8 h. Then it was allowed to cool to room temperature and filtered through a 0.45 µm filter. The filtrate was diluted to 5% weight of TiO₂ by the addition of water. Then solution was placed into a high-pressure autoclave at 220 °C for 12 h. After centrifugation, the aqueous phase was decanted and the solid residue was rinsed with ethanol twice. The aggregates were broken up using an ultrasonic bath and the solvent was removed. The nanoparticles were dissolved in a solution of terpineol containing 5% of ethylcellulose and the paste was homogenised by ball milling. The TiO₂ nanoparticle crystallinity was characterized by X-ray powder analysis confirming the presence of 95% of anatase and 5% of brookite TiO₂ phase.

Alumina nanoparticles synthesis

Al₂O₃ was prepared using a commercial water based solution of Al₂O₃ nanoparticles with uniform diameter of 20 nm (Alfa-Aesar).

Spectroscopic characterization techniques

The UV-visible spectra were recorded using a Shimadzu UV-1700 spectrophotometer. When the absorption spectrum was recorded for dye sensitised films we used the same film without dye to measure the instrument blank and ensure that the light scattering effects had been minimised. For the steady-state fluorescence emission spectra we used an Aminco-Bowman Series 2 fluorimeter with adequate support for solid samples.

Time correlated single photon counting (TCSPC) experiments were carried out with a Lifespec-red picosecond fluorescence lifetime spectrophotometer from Edinburgh Instruments equipped with lasers as excitation sources. The instrument response was always shorter than 300 ps measured at full width half maximum (FWHM).

The transient absorbance experiments were recorded using a home-built system as reported before.¹¹

¹H- and ¹³C-NMR spectra were recorded with a Bruker Avance 400 Ultrashield NMR spectrometer, equipped with a BBI (broadband inverse) probe for proton spectra and a BBO (broadband observe) probe for carbon spectra.

FT-IR spectra were recorded using a FT-IR ThermoNicolet 5700 spectrometer with solid-state samples.

MS spectra were recorded with a Waters LCT Premier, which operates with a Bruker Autoflex instrument. The ionization technique was matrix assisted laser desorption/ionization (MALDI) and the mass was measured by the time of flight (TOF) method.

Materials characterization

The mesoporous nanocrystalline titanium dioxide films were characterised by scanning probe microscopy techniques.

Scanning electron microscopy (SEM) images were obtained using a JEOL JSM 6400 microscope. Before the measurements, the samples were covered with a thin layer of gold to increase the conductivity for superior image quality. Molecular Imaging Pico SPMII apparatus was used to obtain atomic force microscopy (AFM) images. Transmission electron microscopy (TEM) measurements were performed with a JEOL 1011 microscope. The surface analysis was carried out with an Autosorb 1-MP Quantachrome apparatus and the X-ray power diffraction measurements were acquired with a Bruker Siemens Smart CCD diffractometer.

Electrochemical and device characterization

The photoelectrochemical measurement were carried out with a ORIEL 150 W xenon light source equipped with the correct set of filters to achieve the solar spectrum AM 1.5 G. The light intensity was adjusted to 100 mW cm⁻², the equivalent of 1 sun, using a calibrated Si photodiode. The applied potential and cell current were measured with a Keithley model 2600 digital source meter. The current to voltage (*I-V* curve) was measured automatically with home-built Labview software. The charge extraction and photovoltage decay were carried out with a system set-up as previously reported by O'Regan *et al.*¹² using a CHI Instruments model 600B potentiostat-galvanostat which was used for the cyclic voltammetry experiments too.

Device preparation

Nanocrystalline TiO₂ (19 nm particle size) was deposited onto a FTO conducting glass substrate (Hafordt glass TEC 15 Ω cm⁻² resistance) by the well known doctor blade technique. The resulting thickness was 4 µm and the device active area was 1 cm². The resulting electrodes were gradually heated under airflow at 325 °C for 5 min, 375 °C for 5 min, 450 °C for 15 min and 500 °C for 15 min. The heated electrodes were soaked into TiCl₄ aqueous solution 0.04 M at 70 °C for 15 min and then washed with ethanol. Electrodes were heated again at 500 °C for 30 min and cooled before dye adsorption. The platinised counter electrode was made applying a drop of 5 × 10⁻³ M of H₂PtCl₆ in 2-propanol dry solution and spreading onto the conducting glass substrate (FTO). The coated glass was heated under airflow at 390 °C for 15 min.

A solution (5 × 10⁻⁴ M) of **FbP1** or **FbP2** in THF was prepared and the film was immersed in the solution at room temperature until desired absorbance values were reached. The sensitised electrodes were assembled by sandwiching the working and the counter electrode using a thin thermoplastic (Surlyn) frame that melts at 100 °C.

The liquid electrolyte was elaborated using 0.6 M of 1-propyl-2,3-dimethylimidazolium iodide (DMPII), 0.025 M of lithium iodide (LiI), 0.04 M of iodine (I₂) in a mixture of acetonitrile and valeronitrile (85 : 15). This electrolyte is denoted AF4.

The cells were filled with the electrolyte through a hole previously made in the back of a platinised counter electrode. Then, the hole was sealed with a thermoplastic polymer and a cover slide glass. Finally, a drop of silver conductive paint was spread at the electrode contacts to increase the conductivity.

Results and discussion

UV-visible measurements

The visible spectra of **FbP2** in solution and on a TiO₂ film are illustrated in Fig. 2. For the **FbP2** dye, we found that after 2 min of sensitisation, a 4 μm thick mesoporous sensitised film shows an “optimised” (less aggregated) visible spectrum with a sharp Soret band ($\lambda_{\text{SORET}} = 415$ nm). The broadening observed between the solid state and solution measurements, as reported before, is mainly due to the adsorption of the molecules onto the mesoporous film and not to the formation of typical aggregates.¹³

In order to compare the adsorption kinetics of both porphyrins, we monitored the change in absorbance at $\lambda = 520$ nm of two identical 4 μm thick TiO₂ films until the absorbance reached a plateau. Fig. 3 shows the adsorption kinetics comparison

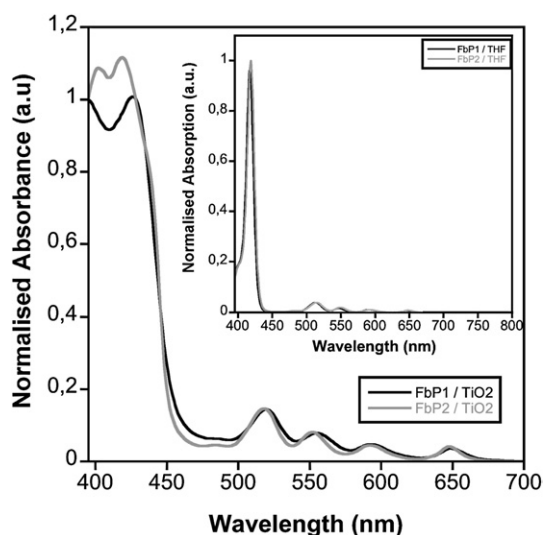


Fig. 2 UV-Vis spectra of **FbP1** (black) and **FbP2** (grey) on a transparent 4 μm thick mesoporous TiO₂ film and in THF solution (inset).

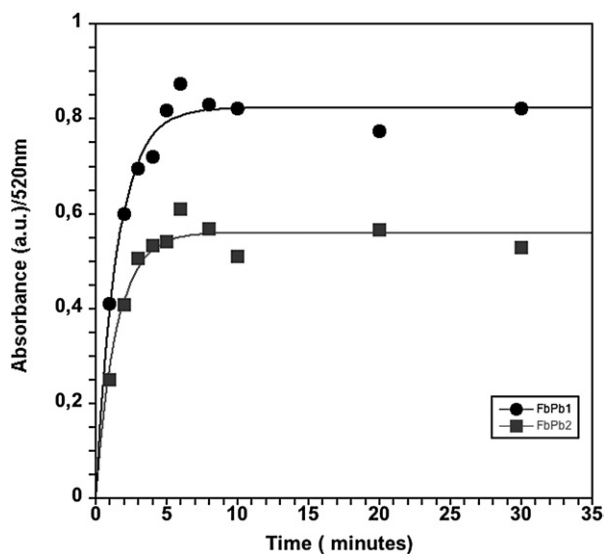


Fig. 3 Absorbance kinetics for **FbP1** (dots) and **FbP2** (squares) on a transparent 4 μm thick mesoporous TiO₂ film at room temperature.

for the films after immersion on a 5×10^{-4} M solution of each dye.

As can be seen in Fig. 3, both films reached different maximum absorbance at 520 nm under the same conditions. In the case of **FbP1** ($\epsilon_{520 \text{ nm}} = 17250 \text{ M}^{-1} \text{ cm}^{-1}$) the film reached a maximum absorbance of 0.8 units while for **FbP2** (with the same $\epsilon_{520 \text{ nm}}$) the maximum absorbance was 0.6 units. This can be understood in terms of porphyrin spatial distribution^{6a} if we take into account that the presence of alkyl chains in **FbP2** implies that the dye occupies a higher surface area at the nanoparticle and also avoids the adsorption of other molecules nearby, preventing the formation of aggregates. Moreover, we also found that the presence of the alkyl chains does not have a large influence over the dye adsorption kinetics. The rate constant for adsorption was studied fitting the experimental adsorption data following the pseudo-first order Lagergren's equation¹⁴ (eqn (1))

$$A = A_{\text{max}}(1 - \exp(-K_{\text{ads}}t)) \quad (1)$$

where A_{max} represents the absorbance maxima and K_{ads} is the rate constant of dye adsorption. For both **FbP1** and **FbP2** K_{ads} was found to be 0.65 min^{-1} . Taking into account these data and the calculated surface area of the TiO₂ films, $99.4 \text{ m}^2 \text{ g}^{-1}$, we have also estimated the porphyrin density in the films: $2.1 \text{ FbP1 nm}^2 \text{ molecule}^{-1}$ and $2.8 \text{ FbP2 nm}^2 \text{ molecule}^{-1}$.

Hence, we can assume that the presence of alkyl groups on the molecule affects the formation of porphyrin aggregates under controlled dye adsorption conditions but does not have a significant influence over the dye adsorption kinetics.

Dye solar cell characterization

We focused our attention on the device performance of **FbP2** using for comparison purposes **FbP1**. We have already demonstrated that the presence of pentyl groups on the porphyrin ring does not really have an influence over the dye adsorption kinetics. However, as can be seen in Fig. 4 the cell characteristics are different.

In both devices the dye adsorption was controlled to achieve the same film absorbance (0.6 a.u. at $\lambda = 520$ nm), which explains the similar photocurrent in both devices despite the presence of alkyl groups in **FbP2**, but more interesting is the fact that the voltage increased too. In spite of this result we decided to study further the different charge transfer processes taking place at the device which have been previously identified in the literature as: (i) electron injection from the dye excited state into the semiconductor conduction band, (ii) electron recombination between the photo-injected electrons and the oxidised dye ($e_{\text{TiO}_2}/\text{dye}^+$), (iii) dye regeneration by the redox active electrolyte ($\text{dye}^*/\text{electrolyte}$) and (iv) electron recombination between the photo-injected electrons and the electrolyte ($e_{\text{TiO}_2}/\text{electrolyte}^+$).

Time correlated single photon counting measurements. The measurement of the excited-state emission lifetime decay of the sensitised films is a straightforward measurement to estimate the electron injection yield of a dye adsorbed onto a semiconductor.¹⁵ As a control sample, a mesoporous wide band-gap metal oxide such as Al₂O₃ is used to prevent electron injection from the excited state since the conduction band of the metal oxide is above

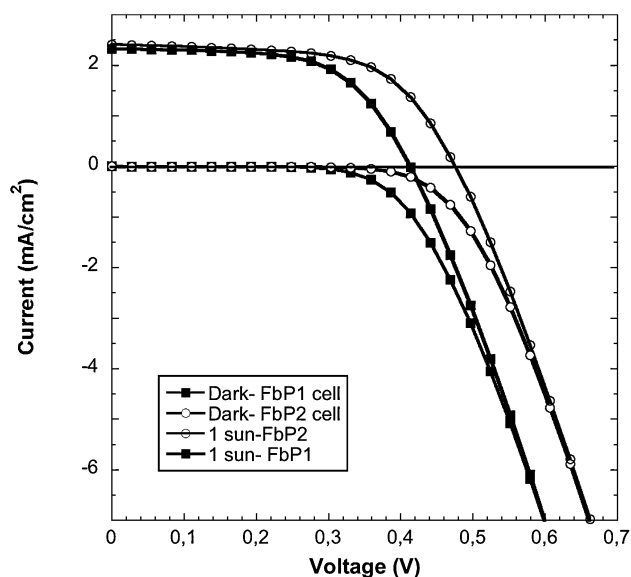


Fig. 4 Current vs. voltage characteristics for 4 μm transparent thick DSSC devices. The cell active area was 1 cm^2 and the electrolyte was AF4.

the LUMO of the molecule. As an example, Fig. 5 shows the emission lifetime measurements for **FbP1** adsorbed onto nanocrystalline mesoporous films of Al_2O_3 and TiO_2 . Both films were sensitized to achieve identical optical absorption (0.6 a.u. at $\lambda = 520$ nm). Under the same measurement conditions (the acquisition time was 900 s) **FbP1** and **FbP2** show almost comparable kinetics. In fact, we would like to note that both on Al_2O_3 transparent mesoporous films or in tetrahydrofuran solvent the kinetics were fitted to identical monoexponential decay.

Further analysis of the emission dynamics reveals that the decays can be also fitted using an extension of the

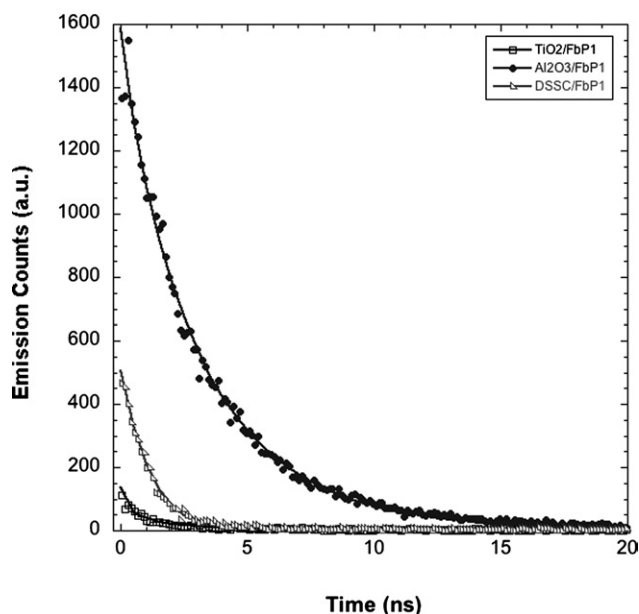


Fig. 5 Time correlated single photon counting measurements for **FbP1** on Al_2O_3 (\bullet), TiO_2 (\square) and a 4 μm thick DSSC with AF4 electrolyte (Δ). The λ_{ex} was 635 nm and the λ_{em} was 720 nm. Acquisition time was 900 s. The curve fits were obtained using eqn (2).

Kohlrausch–Williams–Watts (KWW) function (eqn (2)). As an example **FbP1** sensitised films can be fitted with a monoexponential time of $\tau = 2.95$ ns for Al_2O_3 and a $\tau = 0.67$ ns for TiO_2 while **FbP2** results in $\tau = 3.12$ ns for Al_2O_3 and $\tau = 1.10$ ns for TiO_2

$$\text{decay} \propto \exp[-(t/\tau)^\alpha] \quad (2)$$

Recent work of Koops and Durrant,¹⁶ using DSSC sensitised with ruthenium polypyridyl complexes, proposes that the fitting to the KWW function is consistent with the presence of inhomogeneous broadening of the energetics of electron injection. Moreover, in the case of DSSC sensitised with either **FbP1** or **FbP2** the initial decay amplitude is considerably higher when compared to the TiO_2 sensitised films which is indicative that, in complete devices with redox active electrolyte, the electron injection is much slower in good agreement with the case of ruthenium bis-thiocyanate polypyridyl complexes studied elsewhere.¹⁷ Following the methodology described Koops and Durrant, we estimated that the injection half-time for **FbP1** and **FbP2** occurs in less than 100 ps.

Laser transient absorption spectroscopy (L-TAS). We utilized L-TAS as a technique that allows us to carry out the measurements of the electron recombination dynamics for 4 μm TiO_2 films sensitized with either **FbP1** or **FbP2** in the presence or absence of redox active I_3/I^- electrolyte. The signal decay after the laser pulse is assigned to charge recombination of the dye cation with the electrons in the trap/conduction band states of the TiO_2 semiconductor as reported before (Fig. 6).¹⁸

As expected, all recombination decay dynamics can be fitted to eqn (2) as a consequence of their dependence on the electron trapping/detrapping process at the nanocrystalline TiO_2 particles with $\alpha = 0.42$ for both **FbP1** and **FbP2**. The estimated recombination half time for both porphyrins was in the range of 100–150 μs . From these data it seems difficult to assign the slight differences in electron recombination dynamics between the

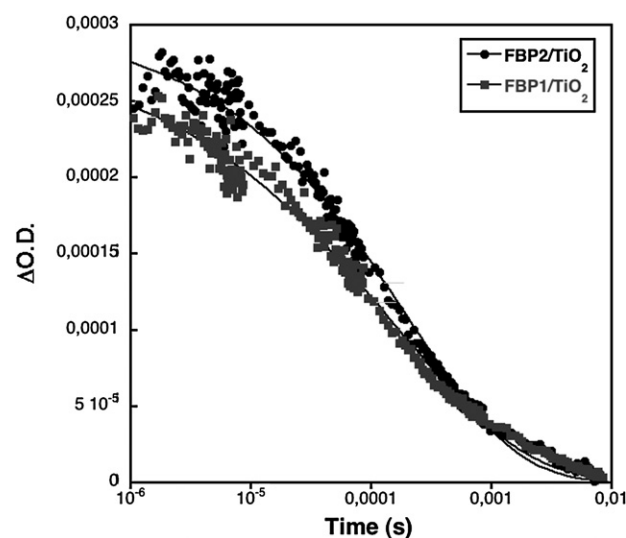


Fig. 6 Electron recombination dynamics for a 4 μm thick dye sensitised mesoporous TiO_2 film. The sensitized film optical absorbance at the laser excitation wavelength ($\lambda_{\text{ex}} = 525$ nm) was 0.3 a.u. for each film. The probe wavelength for the measurement was fixed at $\lambda_{\text{probe}} = 715$ nm.

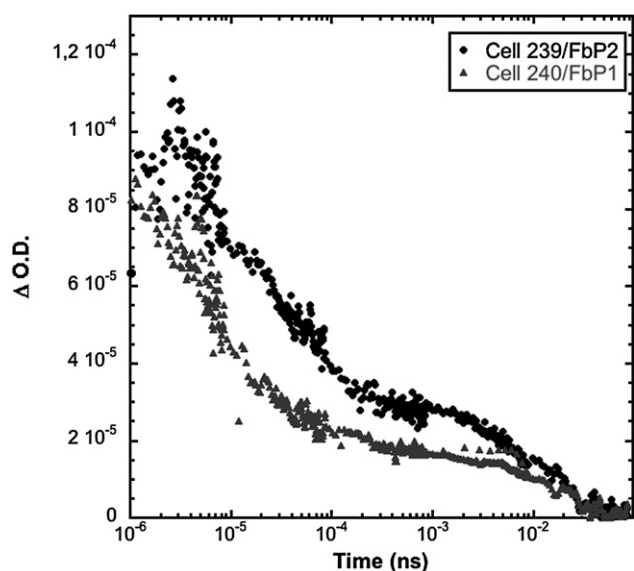


Fig. 7 The electron recombination dynamics for two 4 μm thick DSSCs. The sensitized film optical absorbance at the laser excitation wavelength ($\lambda_{\text{ex}} = 525 \text{ nm}$) was 0.3 a.u. The probe wavelength for the measurements was $\lambda_{\text{probe}} = 715 \text{ nm}$.

dyes and the TiO_2 to the presence of the alkyl chains. In spite of this, we decided to study the electron recombination dynamics in the presence of the redox active electrolyte.

As illustrated in Fig. 7, in the presence of a redox active electrolyte the electron recombination kinetics become biphasic. Previous work¹⁹ demonstrated that the second phase observed in the presence of electrolyte arises from slower formation of by-products as a result of the regeneration of the dye ground state by subsequent electron transfer from the I_3/I^- electrolyte after the electron injection from the dye into the semiconductor conduction band. The fastest component of the optical transient is assigned to the dye cation, which is rapidly regenerated by the electrolyte, and therefore, its lifetime becomes shorter as can be confirmed when compared with the kinetics in Fig. 6, where the signal reaches a plateau at $\Delta\text{O.D.}$ of 2×10^{-4} units while in Fig. 7 the decay has almost disappeared at times shorter than 1 μs . Attending to the results detailed above, we can conclude that in both devices the electron regeneration dynamics compete efficiently with the $\text{TiO}_2/\text{dye}^+$ electron recombination process under the cell operating conditions and the presence of hydrophobic pentyl groups on the porphyrin ring does not affect significantly the kinetic competition between the $\text{TiO}_2/\text{dye}^+$ recombination dynamics and the dye^+/I^- regeneration reaction.

Transient photovoltage measurements. Recently, several authors have employed transient photovoltage measurements, also known as V_{oc} decays, to evaluate the electron recombination dynamics between the photo-injected electrons at the TiO_2 and the oxidised electrolyte.²⁰ For DSSC employing liquid redox electrolytes, such dynamics generally occur on the millisecond time scale and, therefore, no longer compete with the regeneration reaction studied above. On the other hand, it is worth noting that V_{oc} decays are measurements strongly dependent on the accumulated charge at the semiconductor (charge density), and hence to obtain a fair comparison of the $e_{\text{TiO}_2}/\text{electrolyte}^+$ recombination

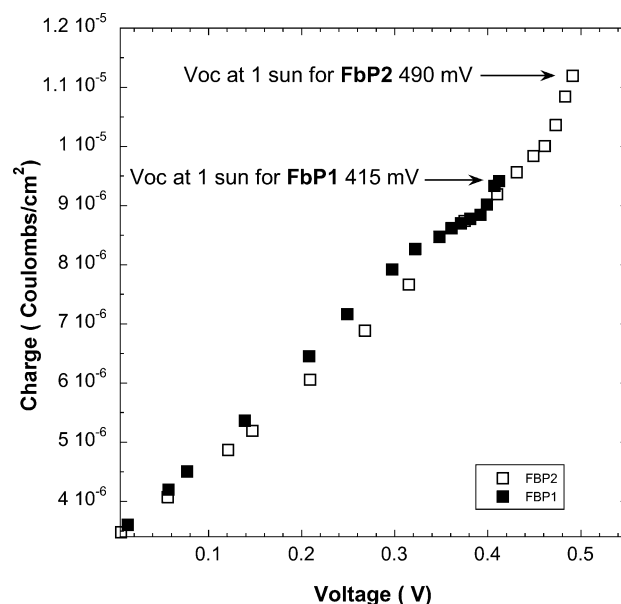


Fig. 8 Charge density as a function of V_{oc} for 4 μm DSSCs sensitized with **FbP1** and **FbP2**. The electrolyte was AF4. Measurements performed at 1 sun.

dynamics between different devices the charge density on both cells must be equal. As illustrated in Fig. 8, in our case, this condition is achieved when the cell voltage is 415 mV.

As can be seen in Fig. 8 for DSSCs sensitized with both **FbP1** and **FbP2** the experimental points emerge along the same curve. Note, as indicated on the figure, that the cells have different V_{oc} when illuminated at 1 sun as expected from the results illustrated before (Fig. 4). The differences in voltage may be due to: (a) a shift on the TiO_2 conduction band with respect to the electrolyte potential or (b) differences in the $e_{\text{TiO}_2}/\text{electrolyte}^+$ recombination reaction. The former hypothesis can be discarded because a change in the TiO_2 conduction band position also implies a shift in the cell charge density as demonstrated previously by other authors.¹⁹ In our case, the hydrophobic pentyl group on **FbP2** does not shift the curve, thus, the differences in voltage must be due to the increase in the $e_{\text{TiO}_2}/\text{electrolyte}^+$ recombination reaction in **FbP1**.

Fig. 9 shows the V_{oc} decay for both devices measured at the same charge density ($V_{\text{oc}} = 415 \text{ mV}$). It is noticeable that the presence of the pentyl groups on the free-base tetra-phenyl porphyrin (**FbP2**) results in slower recombination dynamics between the photo-injected electrons at the TiO_2 and the AF4 electrolyte. We would like to mention that although the measurements were performed on sensitized films with the same absorbance (0.6 a.u. at $\lambda = 520 \text{ nm}$) and, thus, we could expect that the lack of complete coverage would also play an important role in the accelerated recombination dynamics, experiments performed using complete full-monolayer coverage, according to Fig. 3, showed identical performance.

Conclusions

It can be concluded from our studies that the presence of hydrophobic alkyl chains on the molecular structures of porphyrins decreases the recombination between the photo-injected electrons at the TiO_2 nanoparticles and the electrolyte. However,

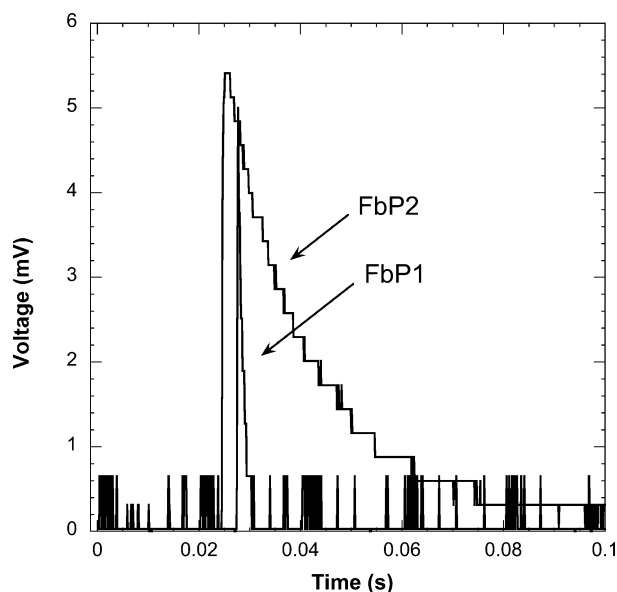


Fig. 9 Photovoltage transients for two 4 μm DSSCs sensitised with **FbP1** and **FbP2**. The electrolyte was AF4.

their presence does not have a severe influence on the adsorption kinetics, and it suggests that they have little influence over the electron recombination between the photo-injected electrons at the TiO_2 nanoparticles and the oxidized porphyrin. This is in good agreement with the “distance-dependence” electron recombination theory,²¹ if we consider that the highest occupied molecular orbital (HOMO) in the porphyrins is delocalized on the aromatic ring, which implies that the distance between the HOMO of the oxidised porphyrin and the surface of the TiO_2 nanoparticles must be identical.²² Moreover, both porphyrin dyes showed almost identical decays for electron recombination and electron regeneration dynamics in the presence of an active redox couple. This implies that the presence of the alkyl chain does not affect the regeneration reaction, which is key for the efficient performance of the devices. The yields of regeneration products are similar with and without the presence of hydrophobic alkyl chains, and the regeneration occurs before the $e_{\text{TiO}_2}/\text{dye}^+$ recombination takes place. However, the analysis of the photovoltage transients revealed that, in fact, the effect of the hydrophobic alkyl chains on the free base porphyrin is to slow the electron recombination dynamics between the photo-injected electrons at the semiconductor and the oxidised electrolyte. The control of this wasteful reaction is key for improving the performance of the DSSC and requires careful attention.

In summary, we have demonstrated using free base porphyrins that the $e_{\text{TiO}_2}/\text{electrolyte}^+$ recombination can be tuned by molecular engineering of the dyes and its consequences at the molecular level have important implications for the device efficiency.

Acknowledgements

EMF and MP thanks the Spanish MEC for a Juan de la Cierva Fellowship and a Ph.D. grant respectively. EP and AF also thank the MEC for the CONSOLIDER-HOPE 0007–2007 project and OrgaPVNet FP6 EU project. PB and MAS thank Dirección General de Investigación, Ministerio de Ciencia y

Tecnología (CTQ2005-08989C01-C02/BQU and CSD2006-0003), Generalitat de Catalunya DURSI (2005SGR00108) and ICIQ Foundation for financial support.

References

- 1 B. O'Regan and M. Grätzel, *Nature*, 1998, **353**, 737.
- 2 (a) M. Grätzel, *Inorg. Chem.*, 2005, **44**, 6841; (b) L. Han, N. Koide, Y. Chib, A. Islam, R. Komiya, N. Fuke, A. Fukui and R. Yamakada, *Appl. Phys. Lett.*, 2005, **86**, 213501; (c) N. Robertson, *Angew. Chem., Int. Ed.*, 2006, **45**, 2338.
- 3 (a) J. R. Durrant, S. A. Haque and E. Palomares, *Chem. Commun.*, 2006, 3279; (b) D. Gust, T. A. Moore and A. L. Moore, *Acc. Chem. Res.*, 2004, **34**, 40; (c) H. Imahori, Y. Mori and Y. Matano, *J. Photochem. Photobiol., C: Photochem. Rev.*, 2003, **4**, 51.
- 4 (a) M. S. Choi, T. Yamazaki, I. Yamazaki and T. Aida, *Angew. Chem., Int. Ed.*, 2004, **43**, 150; (b) S. J. Lee and J. T. Hupp, *Coord. Chem. Rev.*, 2006, **250**, 1710; (c) F. R. Kelley, R. H. Goldsmith and M. R. Wasielewski, *J. Am. Chem. Soc.*, 2007, **129**, 6384.
- 5 (a) W. M. Campbell, K. W. Jolley, P. Wagner, K. Wagner, P. J. Walsh, Ke. C. Gordon, L. Schmidt-Mende, Md. K. Nazeeruddin, Q. Wang, M. Grätzel and D. L. Officer, *J. Phys. Chem. C*, 2007, **111**, 11760; (b) S. Eu, S. Hayashi, T. Umeyama, A. Oguro, M. Kawasaki, N. Kadota, Y. Matano and H. Imahori, *J. Phys. Chem. C*, 2007, **111**, 3528; (c) J. Rochford, D. Chu, A. Hagfeldt and E. Galoppini, *J. Am. Chem. Soc.*, 2007, **129**, 4655; (d) J. R. Stromberg, A. Marton, H. L. Kee, C. Kirmaier, J. R. Diers, C. Muthiah, M. Taniguchi, J. S. Lindsey, D. F. Bocian, G. J. Meyer and D. Holten, *J. Phys. Chem. C*, 2007, **111**, 15464; (e) M. Tanaka, S. Hayashi, S. Eu, T. Umeyama, Y. Matano and H. Imahori, *Chem. Commun.*, 2007, 2069.
- 6 (a) S. Cherian and C. C. Wamser, *J. Phys. Chem. B*, 2000, **104**, 3624; (b) F. Odobel, E. Blart, M. Lagree, M. Villieras, H. Boujtitia, N. El Murr, S. Camaroni and C. A. Bignozzi, *J. Mater. Chem.*, 2003, **13**, 502; (c) J. Jasieniak, M. Johnston and E. R. Waclawik, *J. Phys. Chem. B*, 2004, **108**, 12962.
- 7 A. Kay and M. Grätzel, *J. Phys. Chem.*, 1993, **97**, 6272.
- 8 (a) J. E. Kroeze, N. Hirata, S. Koops, Md. K. Nazeeruddin, L. Schmidt-Mende, M. Grätzel and J. R. Durrant, *J. Am. Chem. Soc.*, 2006, **128**, 16376; (b) L. Schmidt-Mende, J. E. Kroeze, J. R. Durrant, Md. K. Nazeeruddin and M. Grätzel, *Nano Lett.*, 2005, **5**, 1315.
- 9 S. N. Mori, W. Kubo, T. Kanzaki, N. Masaki, Y. Wada and S. Yanagida, *J. Phys. Chem. C*, 2007, **111**, 3522.
- 10 J. S. Lindsey, H. C. Hsu, I. C. Shreiman, P. C. Kearney and A. M. Marguerettaz, *J. Org. Chem.*, 1987, **52**, 827.
- 11 E. Palomares, J. N. Clifford, S. A. Haque, T. Lutz and J. R. Durrant, *J. Am. Chem. Soc.*, 2003, **125**, 475.
- 12 B. C. O'Regan, S. Scully, A. C. Meyer, E. Palomares and J. R. Durrant, *J. Phys. Chem. B*, 2005, **109**, 4616.
- 13 (a) T. Ma, K. Inoue, H. Noma, K. Yao and E. Abe, *J. Photochem. Photobiol., A: Chem.*, 2002, **152**, 207; (b) M. Cervaldo, F. Fungo, E. N. Durantini, J. J. Silber, L. Sereno and L. Otero, *J. Phys. Chem. B*, 2005, **109**, 20953.
- 14 G. Annadurai, M. Chellapandian and M. R. V. Krishnan, *Environ. Monit. Assess.*, 1999, **59**, 111–119.
- 15 Y. Tachibana, I. V. Rubtsov, I. Montanari, K. Yoshihara, D. R. Klug and J. R. Durrant, *J. Photochem. Photobiol., A: Chem.*, 2001, **142**, 215.
- 16 S. Koops and J. R. Durrant, *Inorg. Chim. Acta*, 2008, **361**, 663.
- 17 S. A. Haque, E. Palomares, M. B. Cho, A. N. M. Green, N. Hirata, D. R. Klug and J. R. Durrant, *J. Am. Chem. Soc.*, 2005, **127**, 3456.
- 18 Y. Tachibana, S. A. Haque, I. P. Mercer, J. R. Durrant and D. R. Klug, *J. Phys. Chem. B*, 2000, **104**, 1198.
- 19 I. Montanari, J. Nelson and J. R. Durrant, *J. Phys. Chem. B*, 2002, **106**, 12203.
- 20 (a) B. C. O'Regan and J. R. Durrant, *J. Phys. Chem. B*, 2006, **110**, 8544; (b) A. Zaban, M. Greenshtein and J. Bisquert, *ChemPhysChem*, 2003, **4**, 859.
- 21 J. N. Clifford, E. Palomares, Md. K. Nazeeruddin, M. Grätzel, J. Nelson, X. Li, N. J. Long and J. R. Durrant, *J. Am. Chem. Soc.*, 2004, **126**, 5225.
- 22 O. Cramariuc, T. I. Hukka and T. T. Rantala, *Chem. Phys.*, 2004, **305**, 13.